Robust Design of Electrospray Emitters

Alex A. Gorodetsky*, Collin B. Whittaker†, Audelia Szulman‡, and Benjamin Jorns§
University of Michigan, Ann Arbor, Michigan, 48109

We utilize the Electrospray Propulsion Engineering Toolkit (ESPET) to perform simulation-based design of electrospray emitters. Our design goals are to achieve robust performance of a geometrically feasible design under uncertainties inherent in manufacturing tolerances, model parameters, and operating conditions. We first describe our modeling approach by deriving and justifying geometric, operational, and performance constraints that define a feasible design. We then describe the uncertainties with respect to which we seek robustness. Finally, we describe a rejection sampling algorithm to automate the process of obtaining feasible robust designs that meet constraints with 95% probability. The resulting feasible design space is shown to be smaller and more constrained than designs which meet constraints at fixed, nominal parameter settings.

I. Nomenclature

r_p	=	Pore size
d	=	(Emitter) tip-to-extractor distance
R_c	=	Cone radius of curvature
α	=	Emitter half angle
h	=	Emitter height
R_a	=	Radius of the aperture
$A_{emission}$	=	Active emission area of the cone
N_{pores}	=	Number of pores
P	=	Porosity
θ_d	=	Divergence angle
r_b	=	Emitter base radius
V_0	=	Onset voltage
r_{base}	=	Characteristic size of the emission site
γ	=	Surface tension of the fluid
ϵ_0	=	permittivity of free space
A_{Taylor}	=	average area for an emission site
N_e	=	A scaling factor
r_{pool}	=	Pooling radius
V	=	Voltage
l	=	Minimum distance along the emitter curve to the aperture
BD	=	Breakdown voltage
T	=	Thrust
I_{sp}	=	Isp
η	=	Efficiency
p	=	Pitch
TD	=	Thrust density
T_p	=	Propellant temperature
$C_{R,Limit}$	=	Pure ionic mode transition value
b_0	=	Initial liquid pool radius
N_{spe}	=	Number of sites per emitter

*Assistant Professor, Department of Aerospace Engineering, AIAA Member
†PhD Candidate, Department of Aerospace Engineering, AIAA Student Member
‡Student, Department of Aerospace Engineering
§Assistant Professor, Department of Aerospace Engineering, AIAA Associate Fellow

$C_{R,m}$ = VI slope parameter for pure ionic mode
P_{scale} = Pressure factor

II. Introduction

While electrospray thrusters have potentially game-changing performance for in space applications [1], historically they have been limited in terms of achieved power and thrust levels. This limitation stems from the fact that the active element for these systems, the individual emitter, operates on the micro-scale with a correspondingly small (< 1 uN) level of thrust. To increase performance to thrust levels competitive for small to medium size spacecraft it is necessary to operate tens of thousands of electrosprays concurrently [2].

This need to generate thousands or tens of thousands of emitters invites a fundamental question on the reliability of any arrayed architecture. Indeed, several practical design considerations— type of emitter, manufacturing tolerance, and material choice— all can adversely impact both performance and lifetime when multiplexed [3]. For single fault tolerant systems, it has been shown that even small deviations in individual emitter shape from the nominal design can contribute to substantial reductions in lifetime [4]. Faced with the inherent technical challenges that stem from the need to multiplex, there is a pressing need to identify robust emitter configurations capable of maintaining performance and lifetime.

Numerical methods, in principle, offer a versatile and expedient method for identifying robust emitter configurations. Provided the underlying models are accurate, these tools allow users to parametrically explore the emitter design space — e.g. geometry, propellant type, and operating condition—searching for configurations that yield performance metrics consistent with a stipulated series of performance requirements. In turn, by allowing for known uncertainty within manufacturing tolerances, these same designs can be evaluated for robustness—whether they will maintain performance if individual emitter geometries are allowed to vary.

Nevertheless, the efficacy of numerical tools is limited by the fidelity of the underlying physical models. This limitation is particularly problematic for electrospray emitters where there are aspects of operation that remain poorly understood. This model uncertainty translates to reduced confidence in predictions [5, 6], and as a result, numerical tools must demonstrate that a given design is resilient not only to manufacturing uncertainty but also to uncertainty in the underlying models. The goal of this work is to implement a framework for identifying electrospray designs that are robust under both manufacturing and model parameter uncertainty for large-scale multiplexed emitters.

We have leveraged the Electrospray Propulsion Engineering Toolkit [7] to explore array configurations based on a porous emitter substrate with EMI-BF4 as a propellant. In the following, we first discuss our modeling formulation and identify the constraints and performance metrics based on physical requirements. We then discuss an algorithm for exploring design space to identify robust designs. We then describe a rejection sampling approach that can generate robust designs that satisfy constraints with high probability. Finally, we present a collection of robust designs identified using this methodology, and discuss their properties in relation to the design problem.

III. Theory and Methods

In this section we provide an overview of ESPET and describe the design problem.

A. ESPET Overview

The Electrospray Propulsion Engineering Toolkit (ESPET) is a performance estimation tool for propulsive electrospray systems. It incorporates a suite of scaling laws and a database of propellant properties to provide performance predictions for a variety of popular electrospray architectures [8, 9]. For porous emitters, the ESPET QuickSolver (which we work with here) incorporates models to describe the impedance of and propellant flow through the emitter, emission onset (including of multiple sites), a hard mode switch for whether these sites are operating in a pure-ionic or cone-jet regime, and the corresponding ionic and droplet currents for each site. Some of these models, such as the ionic and cone-jet currents, are semi-empirical, with scalings either specified by the user or taken from published data. Our aim is to assess the robustness of a design with respect to uncertainties in such scaling laws.

B. Design Problem Setup

The design problem is specified through a set of design variables, geometric constraints, operating constraints, and performance constraints. Our aim is to determine combinations of design variables that satisfy geometric and

performance constraints under uncertain manufacturing, parameter, and input conditions. Since ESPET is a highly nonlinear solver with many switching modes of operation, the geometric and performance constraints are correspondingly nonlinear and often discontinuous. These facts prohibit significant use of gradient-based optimization approaches. To this end, we model this as a *feasibility problem*, where we simply search for satisfactory designs.

We consider porous cone-type electrospray emitters here, reduced to six design variables. These variables, and their bounds for this work, are provided in Table 1. To obtain geometrically feasible designs that operate within the calibrated range of ESPET's models we must further encode several geometric constraints.

Table 1 Design variables and their bound constraints

Variable	Bounds
Pore size r_p	$[1 \times 10^{-6}, 2 \times 10^{-5}]$ meters
Emitter-to-extractor dist d	$[1 \times 10^{-6}, 5 \times 10^{-3}]$ meters
Radius of curvature R_c	$[1 \times 10^{-5}, 1 \times 10^{-4}]$ meters
Emitter half angle α	$[15, 60]$ degrees
Emitter height h	$[1 \times 10^{-6}, 1 \times 10^{-2}]$ meters
Radius of the aperture R_a	$[1 \times 10^{-5}, 1 \times 10^{-2}]$ meters

1. Geometric constraints

The first geometric constraint provides a lower bound for the emitter height h. The rounded conical emitter structure considered here, shown in Fig. 1, implies a lower bound that depends on the tip radius of curvature R_C and emitter half angle α:

$$h > R_c \left(1 - \cos\left(\pi/2 - \alpha\right)\right). \tag{1}$$

That is, the absolute minimum height of an emitter is that of the tip (modeled as a spherical cap).

The second geometric constraint relates the pore radius of the medium r_p to the emitter radius of curvature. In particular, we need to ensure that there are some minimum number of pores that can fit on the emitter to prevent the pores from being unphysically large on the scale of the tip. We consider a layer of thickness $2r_p$ immediately below the surface of the active area of the cone, $A_{emission}$. Assuming there are N_{pores} pores in this layer, we can relate the geometry to the porosity (percent void volume) of the substrate P (which we set to $P = 0.48$),

$$\frac{N_{pores} \frac{4\pi}{3} r_p^3}{A_{emission} 2 r_p} = P. \tag{2}$$

ESPET assumes that the active area of the emission site is that of the spherical cap,

$$A_{emission} = 2\pi R_c^2 \left(1 - \cos\left(\pi/2 - \alpha\right)\right). \tag{3}$$

Substituting into Eq. 2 and solving for N_{pores}, we find

$$N_{pores} = 3P \left(\frac{R_c}{r_p}\right)^2 \left(1 - \cos\left(\pi/2 - \alpha\right)\right). \tag{4}$$

We can solve this equation assuming that N_{pores} is a lower bound on the number of pores to obtain an upper bound for the pore radius in terms of the porosity, emitter half angle, and the radius of curvature.

$$r_0 < \left(\frac{3}{N_{pores}} P \left(1 - \cos\left(\pi/2 - \alpha\right)\right)\right)^{1/2} R_c \tag{5}$$

We see that larger pore radii are permitted for larger radius of curvature of the cone, porosity, and half angle. We also add a heuristic constraint to ensure that the pore radius is at least ten times smaller than the radius of curvature,

$$10\, r_p < R_c. \tag{6}$$

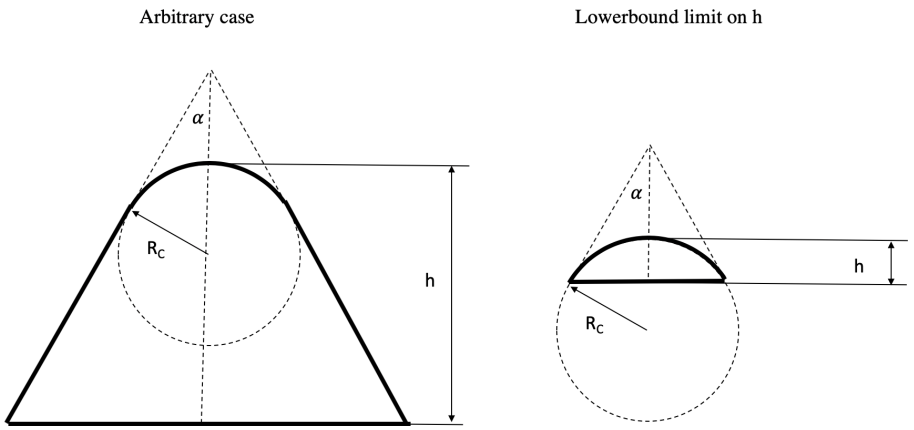

Fig. 1 Side view for cone geometry for porous emitter in the arbitrary and limiting cases

Next we provide lower and upper bound constraints on the radius of the extractor aperture R_a. The lower bound is determined by assuming that the entirety of the spray is contained within a nominal beam divergence angle of θ_d, set to 30 degrees, and ensures that the aperture is sufficiently large to avoid interception of the beam by the extractor, yielding

$$R_a > d \tan \theta_d. \tag{7}$$

The upper bound is to maintain extractor integrity (i.e. that apertures do not intersect). Assuming a worst case (for the apertures) that emitters are packed base to base, the aperture cannot be greater in width than the cone base. The emitter base radius can be computed as

$$r_b = R_c \sin(\pi/2 - \alpha) + (h - R_c(1 - \cos(\pi/2 - \alpha))) \tan(\alpha), \tag{8}$$

So that we have

$$R_a < r_b. \tag{9}$$

2. Operating condition constraints

Next we impose two operational constraints on the operating voltage. The first constraint aims to ensure that each emitter has only a single emission site, to discourage potential off-axis spray. We begin by estimating the onset voltage of an emission site as

$$V_0 = \tanh^{-1}(\eta_0)\left(1 - \eta_0^2\right)\sqrt{\frac{a^2\gamma}{\epsilon_0 r_{base}}}, \tag{10}$$

where γ is the surface tension of the fluid, ϵ_0 is the permittivity of free space, r_{base} is the characteristic size of the emission site (i.e. the base radius of a Taylor cone), and we have the following definitions for a and η_0:

$$\eta_0 = (1 + R_c/d)^{-1/2} \qquad a = 2d/\eta_0. \tag{11}$$

Here d is the emitter tip-to-extractor distance and R_c is the radius of curvature of the cone (see Fig. 1). These expressions arise from equating the electric pressure of the applied field to the capillary pressure at the emission site, where the emitter is approximated an equipotential hyperboloid (see Ref. [10]). We then intersect this expression with ESPET's phenomenological scaling (see [8]) for the feature radius r_{base} based on the number of active emission sites of an emitter,

$$r_{base} = b_i = b_0\left[1 - \left(\frac{i-1}{N_{max}-1}\right)^{1/4}\right] + r_0, \tag{12}$$

where r_p is the pore radius of the substrate, $b_0 = r_{pool}$ is a pooling radius by which propellant can expand outside of the pores, i is the number of active sites (an integer value from $i = 1$ to N_{max}) and N_{max} is the maximum number of possible active sites. This shows that as the number of active sites increases, the characteristic size of the emission sites decreases. Correspondingly Eq. (10) indicates that increasing voltages are required to activate additional sites, as has been observed experimentally [8, 11]. The maximum number of sites is estimated as the ratio of the area available for emission $A_{emission}$ (Eq. (3)) and an average area for an emission site A_{Taylor},

$$N_{max} = N_e \frac{A_{emission}}{A_{Taylor}}, \tag{13}$$

where N_e is a scaling factor (taken here as unity). Finally, we obtain

$$A_{Taylor} = \pi \left[\frac{1}{3} \left(r_{pool} + 2r_0 \right) \right]^2. \tag{14}$$

$A_{emission}$ is the area of the spherical cap of the emitter, and A_{Taylor} is based on an empirically-determined weighted average between r_{pool} and r_p.

Returning to Eq. 10, we see now that we can determine a constraint related to the voltage and geometry for ensuring only one site is active. To this end, we first solve this equation for r_{base}. We then note that for any given voltage V, the following upper bound on r_{base} is required to ensure that the corresponding site will not be active

$$r_{base} < \left(\tanh^{-1}\left(\eta_0\right) \left(1 - \eta_0^2\right) \frac{1}{V} \sqrt{\frac{a^2\gamma}{\epsilon_0}} \right)^2, \tag{15}$$

where we have replaced V_0 with V. Returning to Eq. 12, we see that if there are two emission sites, the base radius of the second site (i = 2) will be given by

$$r_{base}(i = 2) = b_0 \left[1 - \left(\frac{1}{N_{max} - 1} \right)^{1/4} \right] + r_0. \tag{16}$$

We substitute this expression into Eq. 15 to find

$$\left(b_0 \left[1 - \left(\frac{1}{N_{max} - 1} \right)^{1/4} \right] + r_0 \right) < \left(\tanh^{-1}\left(\eta_0\right) \left(1 - \eta_0^2\right) \frac{1}{V} \sqrt{\frac{a^2\gamma}{\epsilon_0.}} \right)^2 \tag{17}$$

We can express this in potentially more physically intuitive way as

$$V < \frac{\left(\tanh^{-1}\left(\eta_0\right) \left(1 - \eta_0^2\right) \sqrt{\frac{a^2\gamma}{\epsilon}} \right)}{\sqrt{\left(b_0 \left[1 - \left(\frac{1}{N_{max} - 1} \right)^{1/4} \right] + r_0 \right)}}. \tag{18}$$

The second operational constraint is required to prevent breakdown between the emitter and extractor electrodes (notwithstanding propellant that may be deposited during operation). The radius of the aperture grid R_a is situated (nominally) directly above an emitter, as in Fig. 2. Consider the distance l between the edge of the extractor aperture and a point on the surface of the conical emitter. For simplicity, the emitter and extractor aperture are assumed axisymmetric. We therefore consider only a 2-D slice of the emitter. l is a function of the geometric parameters d, R_a, R_c, and α, but is also a function of position along the curve of the emitter $l = l(\text{position})$. Though the field strength will be modified by the local curvature, to first approximation we can cast a breakdown constraint BD in terms of the emitter voltage V and the *minimum* distance along the curve (which to simplify notation we now call simply l).

$$\frac{V}{l} < \text{BD}. \tag{19}$$

This indicates that the "strongest field" must be less than the "breakdown field."

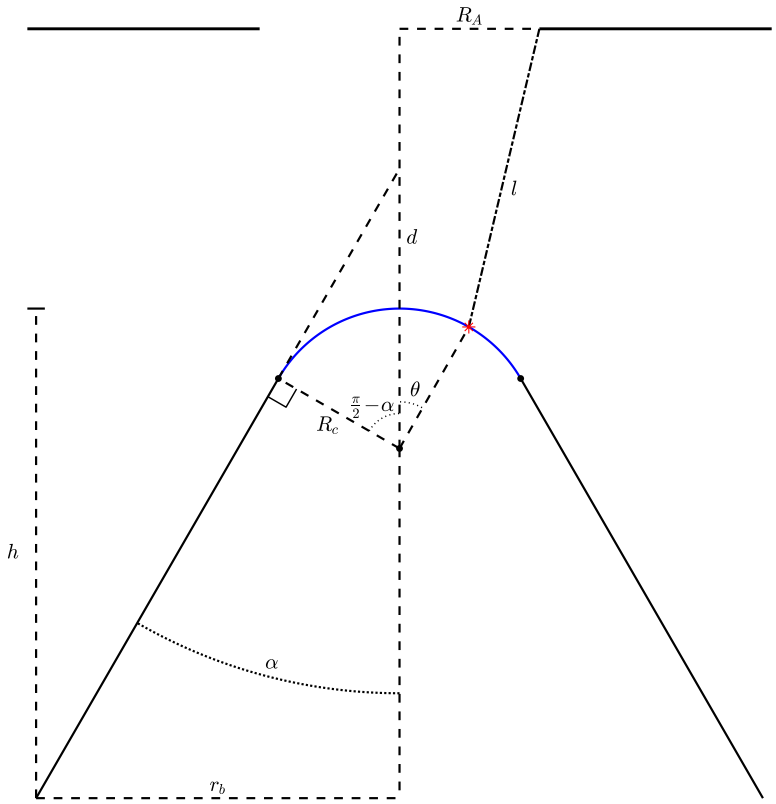

Fig. 2 Side view of conical emitter and extractor electrode

3. Performance constraints

Our performance constraints are designed to satisfy desired thrust, areal thrust density, efficiency, and specific impulse (ISP) characteristics. In terms of the thrust, efficiency, and ISP we seek to satisfy the following minimal conditions (for a single emitter)

$$T > 10^{-7}\ \text{N} \tag{20}$$

$$I_{sp} > 1000\ \text{s} \tag{21}$$

$$\eta > 0.75 \tag{22}$$

To obtain a thrust-density constraint we consider a rectilinear grid of electrospray emitters with pitch p such that the distance between emitter tips along either axis of the grid is p. Equivalently, each emitter can be though of as occupying a square cell of side length p. If the thrust produced by each emitter is T, than the thrust density of the array (not accounting for waste area in the support structure) is T/p^2. Therefore, a constraint on thrust density performance is

$$\frac{T}{p^2} > \text{TD}, \tag{23}$$

such that the achieved thrust density is greater than a target thrust density TD. Maintaining our assumption that emitters are packed base to base (a best case for thrust density), then we can assign

$$p = 2\,r_b, \tag{24}$$

and the constraint (23) above instead becomes

$$\frac{T}{4r_b^2} > \text{TD}, \tag{25}$$

In the subsequent results we use a thrust density lower bound of $TD = 1\ \text{N m}^{-2}$.

C. Uncertainty Specification

In this section we describe the manufacturing and model parameter uncertainties with respect to which we seek robustness. First, we assume that the manufacturing tolerances associated with each design variable are represented as uniform random variables with bounds that are a relative size of 5%. In other words, we assume that the design can be manufactured to within 5% of each of the specified design variables.

The choice of uncertain model parameters can encompass tens to hundreds of parameters, depending upon the complexity of the model. These uncertainties arise because the semi-empirical models in ESPET are typically fit to validation data over certain regimes of operation by tuning scaling laws and creating aggregate parameters representing certain physics. However, existing validation data may be insufficient to accurately tune these parameters for all possible design and operating conditions, and we must account for their uncertainty. Table 2 provides a listing of the set of uncertainties that we have considered. Note that our approach can be flexibly applied to include both other parameters as well as other uncertain representations.

Table 2 Model parameters and associated uncertainties. For a detailed description of these parameters consult the ESPET manual [9]. Each of the parameters is treated as a Uniform random variable with certain lower (lb) and upper (ub) bounds $\mathcal{U}(lb, ub)$. The bounds are chosen as a percentage of nominal values, but the approach is also applicable to other specifications.

Model Parameter	Uncertainty
Propellant temperature T	$\mathcal{U}(280, 360)$K
Pure ionic trans. val. $C_{R,limit}$	$\mathcal{U}(1, 3.25)$
Initial liquid pool radius b_0	$\mathcal{U}(7 \times 10^{-6}, 1 \times 10^{-5})$ meters
Number of sites per emitter N_{spe}	$\mathcal{U}(1, 101)$
VI slope parameter for pure ionic mode $C_{R,m}$	$\mathcal{U}(1.8 \times 10^{-8}, 4.4 \times 10^{-8})$
Pressure factor P_{scale}	$\mathcal{U}(0.023, 0.046)$

IV. Results

In this section we demonstrate both the design methodology and compare robust design to deterministic design under nominal parameters. In both cases, we generate feasible designs through a rejection sampling approach.

In both deterministic and robust cases, we begin by generating a set of design variables to meet geometric constraints. In our context this can be achieved through a procedure whereby variables are sequentially conditioned on previously sampled variables to meet the constraints and all bounds. Specifically, the following ordering is used

1) Uniformly sample the pore size and emitter-to-extractor distance within between the bounds stated in Table 1.
2) Sample the radius of curvature to satisfy the lower bound constraint (6).
3) Sample the emitter cone half angle to satisfy constraint (5).
4) Sample the tip height to satisfy constraint (1).
5) Sample the radius of the aperture to satisfy the constraints (7) and (9).

Note that all these variables must also be sampled to satisfy the bound constraints of Table 1.

Next we use a rejection step to determine whether the sampled design is feasible. For the deterministic assessment, we first fix our parameters at nominal values, and we then use ESPET to evaluate the design performance over an operating voltage range. If the the design satisfies the performance, and only one site is active, then the design is considered feasible. Otherwise, it is rejected. For robustness assessment, we instead perform Monte Carlo sampling over both the parameters according to the distributions provided in Table 2 and 5% manufacturing tolerances around the specified design. We reject the design unless 95% of 100 samples meet the bound, geometric, operating, and performance constraints over some operating voltage range.

Tables 3 and 4 provide summary statistics over the parameters of the feasible design. Moreover, Figure 3 shows the one-d and two-d marginals of the feasible deterministic (blue) and robust (orange) designs. Additionally, a selection of 25 robust designs is displayed in Figure 4. Finally, performance characterizations and visual depictions of the geometries for two of the robust designs can be found in Figures 5 and 6.

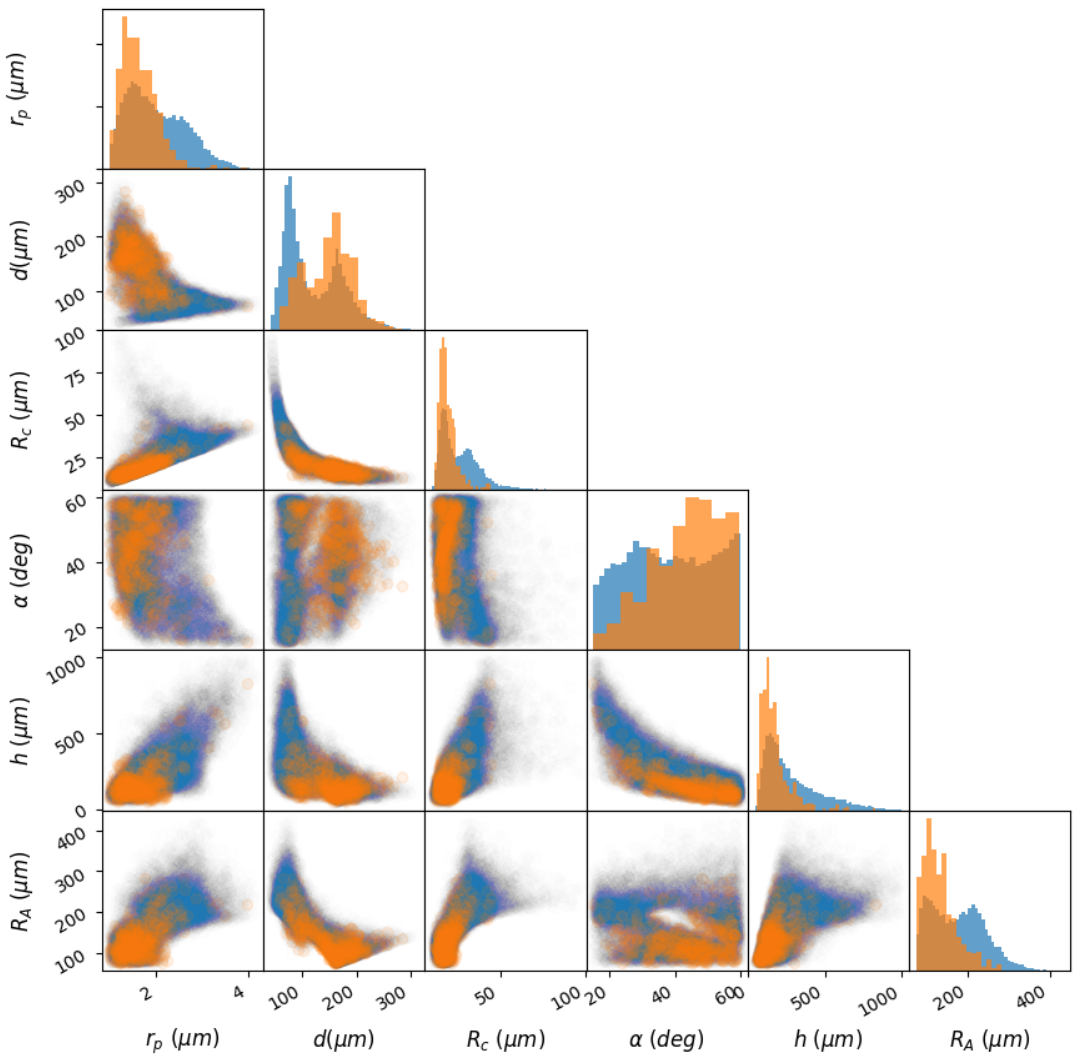

Fig. 3 Comparison of designs satisfying deterministic (blue) and robust (orange) feasibility conditions. Diagonal plots show normalized histograms of the corresponding design variables sampled by the specified procedure. Off-diagonal plots show pair-wise designs. Deterministic designs often have bimodal and heavy-tailed behavior. Robust designs either fully or partially get rid of the bimodality, they also reduce the tails and concentrate in smaller regions.

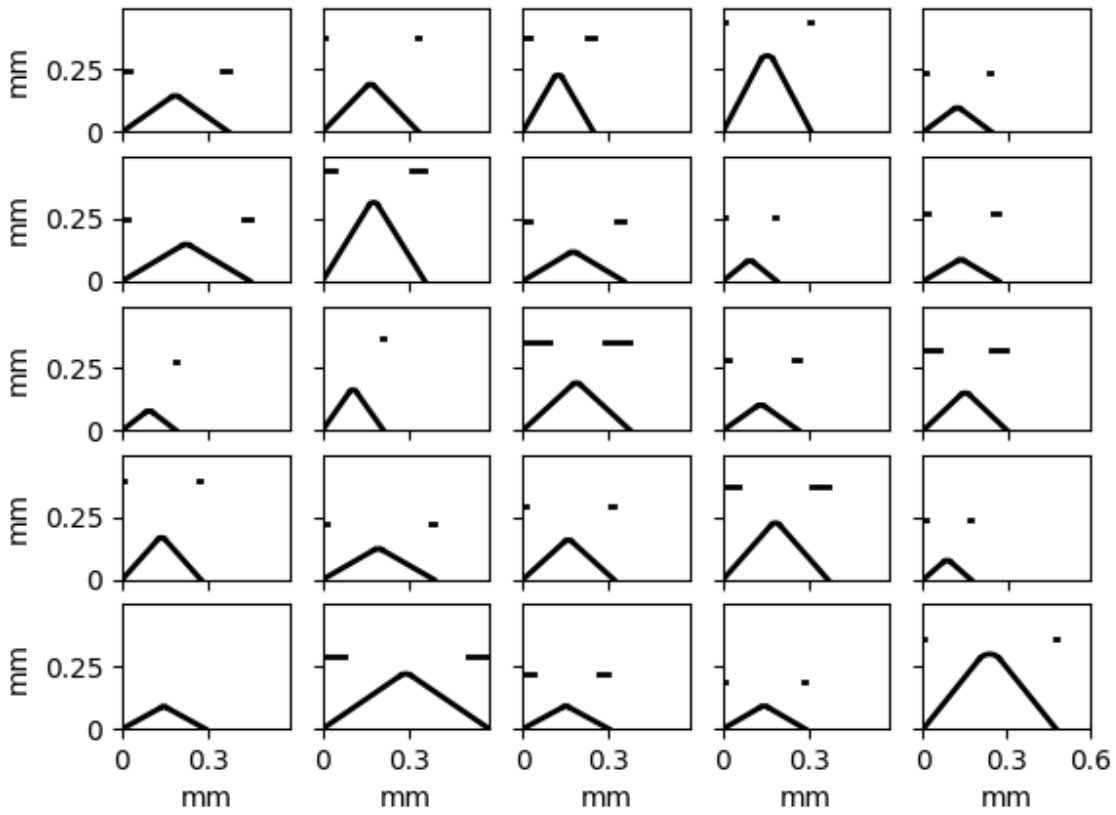

Fig. 4 A visualization of 25 feasible robust designs

Table 3 Statistics (mean, standard deviation, minimum, quantiles, and maximum) of ≈ 16000 designs satisfying deterministic constraints and performances.

Statistic	Pore Radius	Tip-to-Extractor Distance	Radius of Curvature	Half-Angle	Tip Height	Radius of Aperture
mean	2.03E-06	1.19E-04	2.7E-05	38.3	2.87E-04	1.77E-04
std	6.27E-07	5.10E-05	1.2E-05	12.9	1.81E-04	6.4E-05
min	1.00E-06	4.20E-05	1.0E-05	15.0	0.41E-04	7.5E-05
25%	1.52E-06	7.60E-05	1.7E-05	27.4	1.50E-04	1.21E-04
50%	1.92E-06	1.01E-04	2.4E-05	38.1	2.29E-04	1.75E-04
75%	2.49E-06	1.62E-04	3.3E-05	49.7	3.83E-04	2.23E-04
max	4.18E-06	3.12E-04	9.6E-04	60.0	1.00E-03	4.31E-04

Table 4 Statistics (mean, standard deviation, minimum, quantiles, and maximum) of 500 designs that robustly satisfy the constraints.

Statistic	Pore Radius	Tip-to-Extractor Distance	Radius of Curvature	Half-Angle	Tip Height	Radius of Aperture
mean	1.64E-06	1.49E-04	1.9E-05	43.4	1.71E-04	1.32E-04
std	3.95E-07	4.30E-05	5.0E-06	10.6	9.9E-05	4.1E-05
min	1.01E-06	5.80E-05	1.1E-05	15.0	5.1E-05	7.5E-05
25%	1.35E-06	1.15E-04	1.6E-05	36.0	1.11E-04	1.01E-04
50%	1.58E-06	1.53E-04	1.8E-05	45.3	1.46E-04	1.22E-04
75%	1.87E-06	1.80E-04	2.1E-05	52.1	1.97E-04	1.51E-04
max	3.98E-06	2.84E-04	4.4E-05	59.5	8.31E-04	2.83E-04

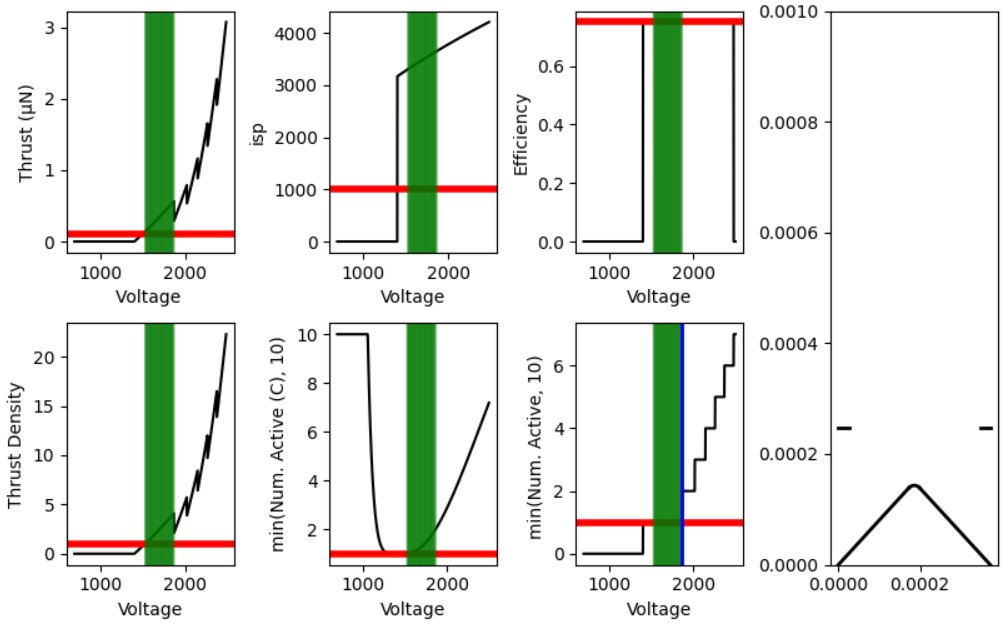

Fig. 5 Example performance of a robust design. Green shaded regions indicate operating regions over which all performance constraints are met. Top row provides thrust, Isp, and efficiency. The bottom row provides thrust density; a continuous relaxation of the active site metric; and the number of active sites visually truncated to a maximum of 10. The right most panel provides a graphical description of the emitter and the extractor.

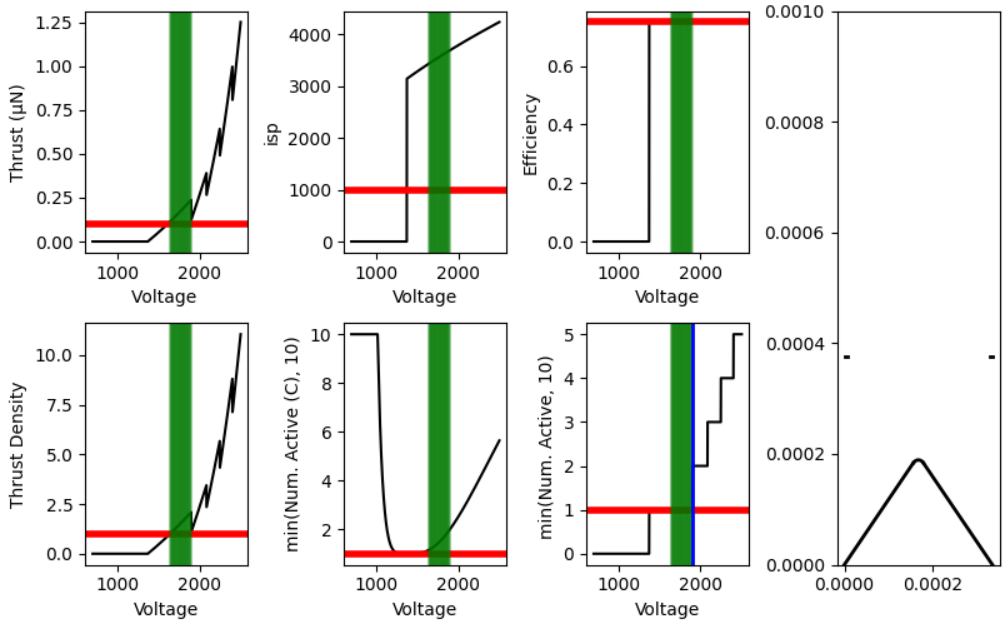

Fig. 6 Another example performance of a robust design. See caption of Fig. 5 for details.

V. Discussion

In this section, we discuss the results. We note that certain design constraints have manifested as visible frontiers within the marginal distributions of Fig. 3. For example, for the 2-d marginal between the curvature radius R_c and the substrate pore radius r_p, we observe a sharp cutoff along a trajectory of positively-correlated R_c and r_p. This corresponds to a boundary beyond which the constraint Eq. (6) is not satisfied. This border actively constrains the design space for both feasible and robust designs. Similar frontiers are readily visible in the 2-d marginals for d and r_p and for R_a and d, and as a result of bound constraints in the 1-d marginal for α. That these constraints are active indicates that our model would likely have permitted unphysical configurations otherwise and could motivate modeling the underlying phenomena in greater detail to capture these limiting process in a less heuristic way.

We also see clearly that robust designs eliminate most of the designs in the tails of the distributions and often eliminate multi-modal sets of feasible deterministic designs. Both the summary statistics and Fig. 3 show that, as expected, the robustness requirement reduces the feasible design space and concentrates it towards the center of the feasible deterministic space. For example, consider that the standard deviation of each design variable is lower for the robust design than for the deterministic design.

We also note that design trades are evident in the figure. For example, the hyperbolic structure in the 2-d marginal of R_c and d is likely a result of field amplification requirements. For instance, as an emitter is moved farther away from the extractor electrode, the electric field at its tip grows weaker — necessitating an increase in the sharpness of the tip to ensure a sufficiently strong field for spray to occur. The fact that there are no feasible designs with both sharp tips and small separations from the extractor is likely a consequence of the operational constraints placed on the voltage, with the high field strengths in this regime either hazarding a breakdown between the electrodes or causing additional emission sites to develop. The ability to concretely assess these interrelationships is an illustration of the power of the proposed design framework. By probing in greater detail these relationships and by closely examining what separates robust designs from their deterministically-feasible counterparts, we can motivate new avenues for modeling, identify dominant sources of uncertainty to inform future experiments, and ascertain which design features are most salient in producing reliable electrospray thrusters.

VI. Conclusion

We have described a model-based design feasibility study for electrospray emitters that determines robust and geometrically feasible designs using the fast ESPET engineering toolkit model. This approach requires the specification of a set of geometric, operational, and performance constraints to ensure valid designs. We also provided a set of designs

that are deemed robust with respect to the stated range of both manufacturing and parameter uncertainties. We showed that these designs reduce the design space compared to that obtained with fixed parameters at nominal values. Future work will experimentally study the robust designs.

Acknowledgments

This work was supported by an Early Stage Innovations grant from NASA's Space Technology Research Grants Program. We thank Mr. Benjamin St. Peter and Dr. Rainer Dressler of Spectral Science, Inc. for their continued work on ESPET and their many illuminating discussions, and Dr. John Yim from NASA Glenn Research Center.

References

[1] Dankanich, J., and Lozano, P., "Dual Mode Green Propulsion for Revolutionary Performance Gains with Minimal Recurring Investments,," *Planetary Science Visison 2050 Workshop*, 2017.

[2] Demmons, N. R., Hruby, V. J., Courtney, D., Ziemer, J. K., and Marrese-Reading, C., *Ground and On-Orbit Thruster Performance Comparison for the Lisa Pathfinder Colloid MicroNewton Thrusters*, American Institute of Aeronautics and Astronautics, 2018. https://doi.org/doi:10.2514/6.2018-4643, URL https://doi.org/10.2514/6.2018-4643.

[3] Krejci, D., Mier-Hicks, F., Fucetola, C., Lozano, P., Schouten, A. H., , and Martel, F., "Design and Characterization of a Scalable ion Electrospray Propulsion System," *34th International Electric Propuls, IEPC-2015-149.*, 2015.

[4] Jorns, B., Gorodetsky, A., Lasky, I., Kimer, A., Dahl, P., St. Peter, B., and A., D., "Uncertainty Quantification of Electrospray Thruster Array Lifetime," *36th International Electric Propulsion Conference, Austria, Vienna*, 2019.

[5] Dahl, P. N., Kimber, A. M., and Jorns, B., *Data-Driven Scaling Laws for Electrospray Plume Divergence from a Capillary Tube*, ???? https://doi.org/10.2514/6.2019-3901, URL https://arc.aiaa.org/doi/abs/10.2514/6.2019-3901.

[6] Whittaker, C. B., Gorodetsky, A., and Jorns, B., *Quantifying Uncertainty in the Scaling Laws of Porous Electrospray Emitters*, ???? https://doi.org/10.2514/6.2020-3615, URL https://arc.aiaa.org/doi/abs/10.2514/6.2020-3615.

[7] St. Peter, B., Dressler, R. A., Chiu, Y.-h., Fedkiw, T., Wang, Y., and Song, H., "Electrospray Propulsion Engineering Toolkit (ESPET)," *35th International Electric Propulsion Conference Georgia Institute of Technology*, 2017, pp. IEPC–2017–206.

[8] St.Peter, B., Dressler, R. A., Chiu, Y.-H., and Fedkiw, T., "Electrospray Propulsion Engineering Toolkit (ESPET)," *Aerospace*, Vol. 7, No. 91, 2020.

[9] Dressler, R. A., and St.Peter, B., *Electrospray Propulsion Engineering Toolkit, ESPET 1.0*, Spectral Sciences, Inc., 2018.

[10] Martinez-Sanchez, M., "Lecture 23-25: Colloidal Engines," Web, 2004. URL https://dspace.mit.edu/bitstream/handle/1721.1/100855/16-522-spring-2004/contents/lecture-notes/lecture23_25.pdf, lecture notes.

[11] Perez-Martinez, C., and Lozano, P., "Ion field-evaporation from ionic liquids infusing carbon xerogel microtips," *Applied Physics Letters*, Vol. 107, No. 4, 2015, p. 043501.